Rotational characterization of seismic events along Chile

A. Acosta-Pizarro[1], D. Pastén[1], and C. Hermann-Avigliano[2]

[1]Departamento de Física, Facultad de Ciencias. Universidad de Chile, Santiago, Chile

[2]Departamento de Física and Millennium Institute for Research in Optic (MIRO), Facultad de Ciencias Físicas y Matemáticas, Universidad de Chile, Santiago, Chile

ABSTRACT

We characterize 117 seismic events occurred in Chile and registered at the Wetzell Geodetic Observatory (BWL-RAS) in Germany in terms of rotational seismic parameters. Using the Minimum Curvature Interpolation method, we create a 2D map with the Vertical Rotation Rate (VRR) divided in three zones from the Chilean Coast: Northern, Central, and Southern area. In order to describe the behavior of VRR along time, we create a timeline and seismic moment model showing events in these areas with different values of VRR. The analyzed data includes four large earthquakes occurred in different zones with magnitudes greater than M_w7.5. We focus our analysis in the values of the rotational velocity for these earthquakes and show that the VRR does not have a clear relation with the seismic moment magnitude. Our results open a new way to describe and study seismic events. It can be useful to generate a deeper understanding of the dynamics in the underlying processes involved in the earthquake occurrence. As well, our results could serve to improve safety regulations in construction and mining, since important rotational movements may be present even within low moment magnitude events.

Keywords: Rotational Seismic Waves, Earthquakes, Chile

1. INTRODUCTION

Chile is located in a seismic active zone in South America. This great activity is produced by the shock between the Nazca plate and the South American plate. During the last 60 years more than 7 earthquakes greater than M_w7.0 have occurred along the Chilean coast, producing significant disasters like the well known event at 1960 in Valdivia, with a magnitude M_w9.5[1] and the event at 2010 in Maule with magnitude M_w8.8.[1,2] In previous articles, almost the complete Chilean coast has been studied by GPS, and the zones with high and low seismic coupling between the plates involved in this shock have been identified.[3,4] This type of analysis allows us to make an overview of the so-called seismic gaps.[5–7] It is known that between two large seismic events within the same region, the plates accumulate strain energy. In Chile we have experienced 4 large earthquakes with magnitudes greater than M_w7.0 from 2010 up to the present along the subduction zone, giving a complex scenario for the

people living there. Although the seismic activity in Chile has been widely studied,[3,4,8] the rotational ground motion has not been considered in those explorations due to the fact that in general it can be neglected against the translational ground motion, which is orders of magnitude larger. Nevertheless, there are small tilt effects embedded in strong-motion earthquakes that cannot be ignored in the processing of seismic data, specially in the calculation of permanent displacements and long-periods.[9]

Two types of surfaces waves propagate along the surface of the Earth: Rayleigh and Love waves. The former result from an interaction of P-waves and SV-waves (vertically polarized) with the free surface, generating an elliptical retrograde ground displacement in the vertical plane. The latter are generated by the interaction of horizontally polarized S-waves with the free surface, generating a horizontal transverse motion. Because of that, Love-waves propagate faster than Rayleigh-waves. In terms of rotational motions, both Loves and Rayleigh waves have non-zero rotational components[10,11] and are dominant features on the seismograms in the range of $10 - 200\,s$. Most of the reliable information (like phase velocities) on the long period part of seismic source spectra is obtained from surfaces waves.[9]

Different sensors have been developed in order to measure rotational ground motion in seismic waves.[12,13] The rotation rates expected and observed in seismology can vary from 10^{-1} rad/s[14,15] for near seismic sources to 10^{-11} rad/s for large earthquakes at teleseismic distances.[9,11] Since this range of possible measurements is extremely wide ($200\,dB$), it is hard to imagine a single instrument capable to run such measurements, and even more unlikely is to imagine a measuring system with resolutions of the order of 10^{-11} rad/s for large earthquakes at teleseismic distances.[13]

However, a relatively new type of sensor based on optical interference patterns has been achieved. Laser-type gyroscopes are optical sensors with the highest sensitivity and the best accuracy for collecting rotational seismic data for both, near the source and teleseismic events.[11]

Such a laser-type giroscope is available in Germany. Since 2001 the G-Ring laser interferometer has been operating at the primary geodetic and seismological station at Wettzel,[12] which belongs to the Rotational Motion for Seismologist project (ROMY).

This G-Ring interferometer sensor has registered at least $17,000$ events around the world and the data is an open database since 2007.[12]

A recent article has shown the impact of the rotational ground motion on the structural response of buildings.[16] In this sense it becomes important to study rotational seismic parameters, in order to establish new knowledge about seismic waves that could allow the optimization and improvement of current seismological models to explore deeper the internal structure of the earth. This new knowledge has the potential to improve

as well civil works within mining, construction, geothermal stations, among others. In this paper we analyze seismic events registered by the Wettzel Geodetic Observatory database (BWLRAS) along the coast of Chile. We characterize rotational parameters for earthquakes occurring within this active seismic zone since 2007 in terms of the Vertical Rotation Rate (VRR). We present our results with the main objective of generating a better understanding of how the rotational velocities could affect the vicinity, and if they are related in any form with the seismic moment magnitude. This characterization is carried out through a $2D$ map of 117 events registered in Chile and a $3D$ time-line and seismic moment modeling, all in terms of the VRR. The paper is organized as follow. We first recall the theory of rotational seismic motions. We then present, in Sec. 3, the methodology of our characterization. We present our characterization results in Sec. 4 and discussions is presented in Sec. 5. We give our conclusions and remarks in Sec. 6.

2. THEORY OF ROTATIONAL SEISMIC MOTIONS

General elasticity theory serves to describe the behavior of seismic waves. We consider an infinitesimally small deformation for a finite-body particle. For displacements of two arbitrary points located at x and $x+\delta x$ we have:[10]

$$u(x+\delta x) = u(x) + \epsilon\delta x + \omega \times x \tag{1}$$

where the terms $\epsilon\delta x$ and $\omega \times x$ are related with the strain and rotation second order tensors respectively. In particular, ω can defined as:

$$\omega = \frac{1}{2}\nabla \times -u(x) \tag{2}$$

the angle of rigid rotation generated by the disturbance. This vector does not enter in the Hooke's law. Eq. 1 illustrates that three components of translation, six components of strain and three components of rotation are needed to fully characterize the change in the medium around point x.

Consider a plane wave propagating transversely through an isotropic and homogeneous media with a displacement given by[10]

$$y\mathbf{U}(\mathbf{x},t) = U\mathbf{p}W(t - \frac{\mathbf{x}\cdot\mathbf{n}}{c}) \tag{3}$$

with U the wave amplitude, $\mathbf{p}$ the polarization, W the normalized wavefront, and $\mathbf{n}$ the wave plane direction moving with a phase velocity c. The expression $(\mathbf{x},t)$ corresponds to (x,y,z,t) vector. From Eq. 3, we can obtain the particle velocity

$$\mathbf{V}(\mathbf{x},t) = U\mathbf{p}\dot{W}(t - \frac{\mathbf{x}\cdot\mathbf{n}}{c}). \tag{4}$$

Then, we can consider a temporal derivative in Eq. 2, to obtain the rotation rate, which is defined as[10]

$$\dot{\Omega}(\mathbf{x},\mathrm{t}) = \frac{1}{2}\nabla\times\mathbf{V} = -\frac{U}{2c}\mathbf{p}\times\dot{W}(t - \frac{\mathbf{x}\cdot\mathbf{n}}{c}). \tag{5}$$

Thus, the divergence $\nabla\cdot\mathbf{V}(\mathbf{x},t)$ is associated with a plane wave as

$$\nabla\cdot\mathbf{V}(\mathbf{x},t) = -\frac{U}{c}\mathbf{p}\cdot\mathbf{n}(t - \frac{\mathbf{x}\cdot\mathbf{n}}{c}). \tag{6}$$

Particularly for a homogeneous medium, the P-wave is free of rotational effects because it is parallel to the polarization. Then $c = V_p$ since $\mathbf{n}\times\mathbf{p} = \mathbf{0}$. On the other hand, the S-wave is orthogonal to the polarization, which means that $\mathbf{n}\cdot\mathbf{p} = \mathbf{0}$ and $\mathrm{c} = \mathrm{V_s}$.

Hence, for an elastic, isotropic, and homogeneous medium, rotational effects are restricted only to S-wave propagation. In other words, if $\dot{\Omega} = 0$ and the divergence is $\neq 0$, the incident wave is P-wave while if $\dot{\Omega} \neq 0$ and the divergence is zero, then the incident wave is an S-wave. This point is important since it tells us that translational motion is not detected by rotational sensors and hence, there is a natural split between P and S waves. The sensor used here is the Ring Laser Gyroscope (RLG), which is based on the Sagnac effect,[17] where two laser beams traveling in a enclosed fiber-optic loop in opposite directions display interference phenomena. When there are rotational motions, phase changes and beat frequencies can be observed between the two counterpropagating beams. Measuring frequencies is much more convenient than measuring phase differences since in can be measured with higher precision. The beat frequency that appears is proportional to the rotational rate[18]

$$\Delta\nu = \frac{4An\dot{\Omega}}{\lambda P} \tag{7}$$

where A is the area inside the interferometer, P is the perimeter of the device, λ the wavelength of the laser, and n is the unit vector perpendicular to the laser ring area.

The sensitivity of such a device can be improved by increasing the number of loops in the interferometer.[19] At the German station, three fiber optic gyroscopes are assembled together with perpendicular normal vectors, to create a 3D-component sensor and hence allowing the measurement of rotational rates in all directions.[20]

Under the assumption of a transversely polarized plane wave, the vertical rotation rate $\dot{\Omega}_z$ (VRR) and transverse acceleration a_t can be combined.[11] In this case, both VRR and a_t are in phase, and the amplitudes are related by

$$\frac{a_t}{\dot{\Omega}_z} = -2c \tag{8}$$

where c is the apparent horizontal phase velocity. In this context, it is also possible to estimate the backazimuth through the correlation between vertical rotation rate and transverse aceleration.

3. METHODOLOGY

We make use of the BWLRAS open database available at ROMY website[12] to obtain rotational parameters. The RLG 4x4 interferometer has a self-noise resolution of $60 \times 10^{-14}(rad/s)Hz^{-1/2}$, which allows to record small (Mw <6.0) teleseismic events at reasonable signal-to-noise ratios (SNRs) as well as Earth's free oscillations. The seismic events measured by the open database are described by the epicenter, the moment magnitude M_w, the date and the depth. These values are obtained by scripts that are fed by quick Centroid Moment Tensor (CMT) solutions provided by the Global CMT catalog,[21] which means that earthquakes locations comes from known seismic catalogues. The rotational parameters are obtained by a time windows that it is selected from the G-ring in order to obtained vertical rotation rate.

The open database has a web interface where waveform data of rotational and translational ground motions can be processed. This database contains the following information

1. Event background information (location, time, date, M_w, latitude, longitude and depth)
2. Vertical rotation rate (VRR), Transverse acceleration.
3. Parameter Estimation: Love−wave phase velocity, back azimuth and P−coda analysis.

Since 2007 to 2018, the BWLRAS has recorded more than 17,000 events around the world. In our paper we use a data set in the range of 0.7−1.0 of cross-correlation (CC)[12] that cover an area between the 18° South Latitude and 42° South Latitude, and between 75° West Longitude and 66° West Longitude, which basically correspond to Chilean coast as shown in Fig. 1. For this analysis we use events with magnitudes between M_w4.5 and M_w8.8. The total number of data analyzed is 117 events.

The database described above has spatial information of rotational seismic events occurred in Chile. Because the location of each events are obtained by a seismic catalogues, no spacial resolution are available. Within this, we estimate the VRR data through an interpolation method in order to construct a contour map representative of each area using the Minimum Curvature (MC) algorithm.[22] This is a fast, versatile interpolation method that produces an optimally smooth surface that is visually appealing for a better interpretation of data. The surface is created over a grid which is defined by the Longitude (X), Latitude (Y) and VRR as shown in figure 2.

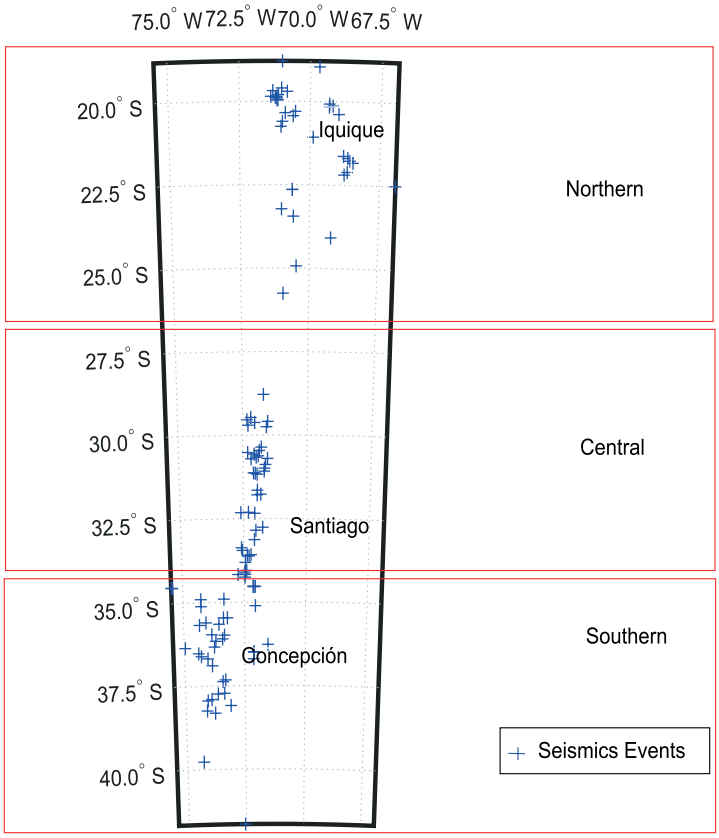

Figure 1: Map of the geographical position of the 117 seismic events along Chile recorded by BWRLAS station since 2007 to 2018 in a range between 0.7 and 1.0 CC. These events include moment magnitudes between $M_w 4.5$ and $M_w 8.8$ in a range of 17 km and 153 km of depth, since 2007 to 2018. The database is separated in three areas: Northern Chile, Central Chile and Southern Chile.

From this database and considering the Latitude, Longitude, date and M_w of the events, we interpolate the VRR in two models. The first is a 3D Timeline Model where the temporal evolution of VRR is studied. The second is a 3D Seismic Moment where the VRR is evaluated against the Mw where the released seismic energy is analyzed in terms of rotational seismic velocities. Both models are created considering the Inverse Distance Weighting (IDW),[23] which is method for multivariate interpolation where the set of data are displayed over a regular mesh and assigned as interdependent variables in terms of the distance between them. All the unknown points are calculated with a weighted average of the values available from the known points.[23]

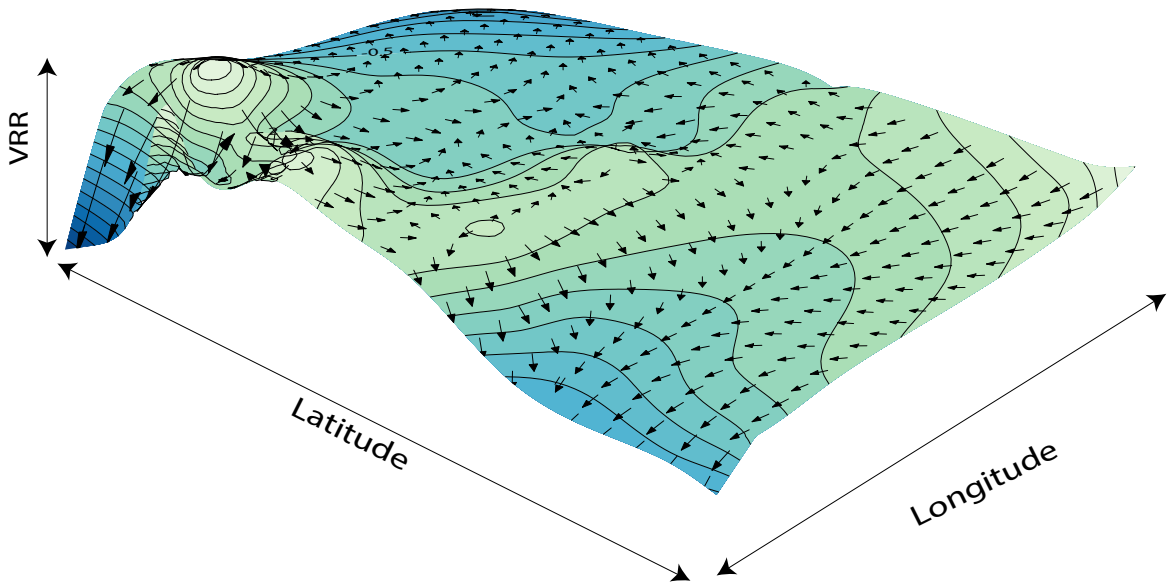

Figure 2: MCI schema used for the interpolation of rotational seismic data. The interpolation occurs when a grid vector (black arrows) fits smooth surfaces (black lines) between a set of data. Each point of the interpolation generates a regular grid which is defined by the dimension of Latitude, Longitude and VRR. The result of this interpolation is a 2D contour map where the contrast of colours correspond to different values of VRR distributed over the map.

We study the correlation between M_w and VRR by using the Spearman Rank (SR) correlation method, which is a robust and consistent non-parametric measure of rank correlation between two statistical variables.[24] It is defined as

$$P_{sp} = 1 - \frac{6\sum_{i=1}^{n} D_i^2}{n(n^2-1)} \tag{9}$$

where D_i is the difference between the rank of two variables.

The SR evaluates the correlation of two variables using a monotonic function. If there are no repeated data values, a perfect Spearman correlation of $+1$ or -1 occurs when each of the variables is a perfect monotone function of the other.

4. RESULTS

The MCI interpolation method is applied to the database at the three areas selected in Fig. 1. The interpolation considers the Latitude and Longitude as the base area. The VRR is interpolated into this area creating a 2D map as shown in Fig. 3. There are 3 maps which correspond to Northern, Central and Southern area of Chile. Each

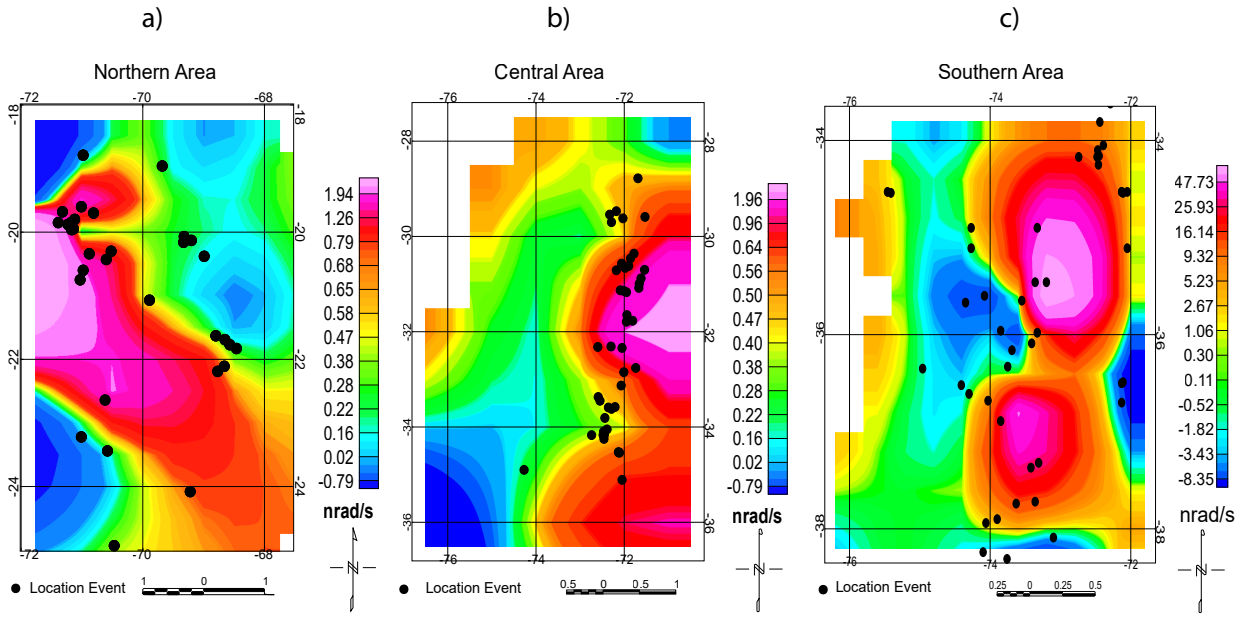

Figure 3: Interpolation of the VRR for the three zones studied in Chile, a) Northern zone, b) Central zone and c) Southern zone. The black triangles show the seismic events registered for each zone by the BWLRAS, between 2007 and 2018. The different values of VRR are representing by the colour scale in the right hand of each maps.

maps were coloured following the normal distribution of data from each area (northern, central and southern) in order to represent the VRR along the map and because of that, the colour legend bar on the right hand at each map is associated with the contour curves.

Fig. 3a) shows peak values of the VRR at 20° South Latitude and 72° West Longitude with a VRR> 1.3 nrad/s. Toward the 23° South Latitude and 69° West Longitude the VRR decreases until 1.0 nrad/s, these spatial positions correspond to intraplate events. In Fig. 3b) there are two zones between the 32° South Latitude and 72° West Longitude with high values of VRR, around 2.2 nrad/s. In Fig. 3c) there are two hot spots of VRR> 60 nrad/s between 34° South Latitude and 38° South Latitude and between 74° West Longitude and 78° West Longitude. In the southern area, Fig. 3c) the higher values of VRR are concentrated in 32° South Latitude and 72° West Longitude with 2.2 nrad/s.

In order to characterize the behavior of VRR in time and to understand how the VRR could be related to M_w for the data set Fig. 1, we compute a 3D timeline and Seismic Moment M_w model using the IDW interpolation method in a voxel. To describe the rotational velocity, we filter the VRR data in order to observe peak values in the Timeline and Seismic Moment. Both filters are shown on the right hand on Figs. 4, 5 and 6.

Fig. 4a) shows 33 events registered at BWLRAS from 2007 to 2018 with a M_w range between 4.1 and 8.2. Fig. 4b) shows a filter in VRR data between 1.3 and 3.57 nrad/s where we observe two main events. The first event is directly related with the large earthquake occurred in Iquique in 2014 with M_w8.2 at 21 km of depth. The second seismic event is related to an event of M_w5.5 occurred at 121 km of depth in the zone of Calama city. Fig. 4c) shows the behavior of VRR as a function of M_w and Fig. 4d) shows a filter of Fig. 4c) in VRR between 1.3 and 3.6 nrad/s. It is possible to identify a seismic event of M_w4.7 with VRR of 1.6 nrad/s and another seismic event of M_w5.5 with VRR of 1.93 nrad/s. Also we can observe the large earthquake of M_w8.2 with 2.8 nrad/s.

Fig 5a) shows 44 seismic events registered by the BWLRAS between years 2007 and 2018 in the Central zone of Chile, with moment magnitudes between M_w5.0 and M_w8.3. Fig. 5b) shows a filter in the VRR for the Fig. 5a) between 2.0 nrad/s and 5.0 nrad/s. Here we observe seismic events occurred along 2016 with a VRR peak value of 3.2 $nrad/s$. Fig. 5c) shows the behavior of VRR as a function of M_w while Fig. 5d) shows a filter between 2.0 and 9.1 nrad/s in Fig. 5c). The last figure shows a seismic event of M_w7.1 occurred at 47 Km North West, close to Los Vilos, with 9.0 nrad/s and the large earthquake in Illapel of 8.3 M_w with a VRR of 9.0 nrad/s.

Fig. 6a) shows 40 seismic events registered by the BWLRAS between years 2007 and 2018 in the Southern zone of Chile, with moment magnitudes between M_w4.9 and M_w8.8. This figure shows a change in the value of the VRR in time. For the M_w8.8 large earthquake in 2010, the value of the VRR had an increase with two events of M_w5.5 and M_w6.6, after this seismic events, the value of the VRR shows a decrease, but the VRR have had an increase from the final of the year 2015. This last increase could have been reflected in the earthquake of M_w7.6 in Chiloé, Southern zone of Chile. Fig. 6b) shows a filter of Fig. 6a) between 30 nrad/s and 149.34 nrad/s, where we observe seismic events that have occurred between years 2010 and 2016 with a VRR peak value of 149.34 nrad/s. Fig. 6c) shows the behavior of VRR as a function of M_w. Fig. 6d) shows a filter of Fig. 6c) in VRR between 30 and 149.34 nrad/s. This last figure shows seismic events of M_w4.9 with a VRR of 30 nrad/s and seismic events of M_w5.5 with a VRR of 87 nrad/s.

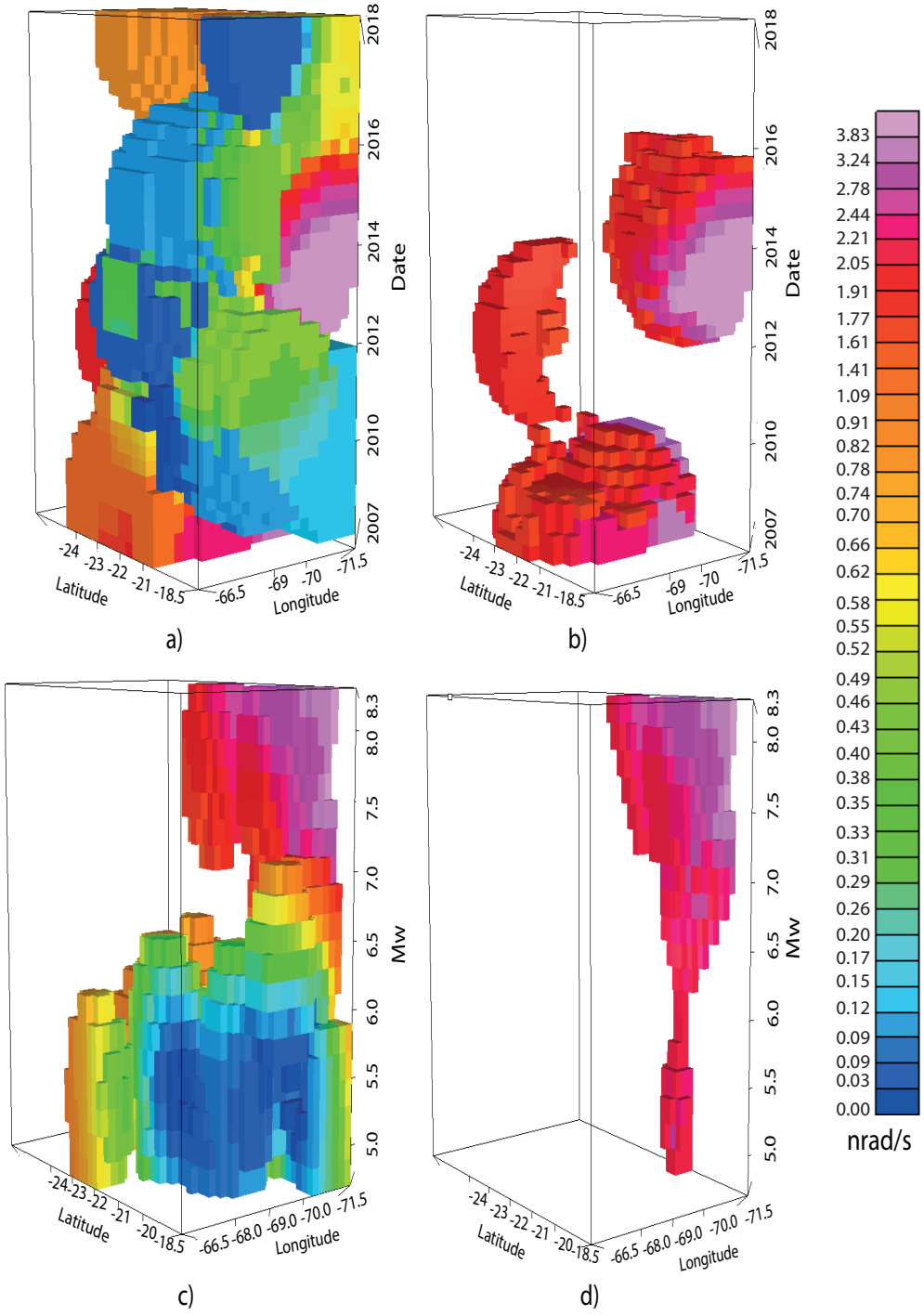

Figure 4: Timeline and Seismic Moment modeling for Northern zone of Chile. Figs. 4a) and 4b) are plotted by Longitude, Latitude and the vertical coordinate is defined by time. In Figs. 4c) and 4d) the vertical coordinate is the seismic moment.

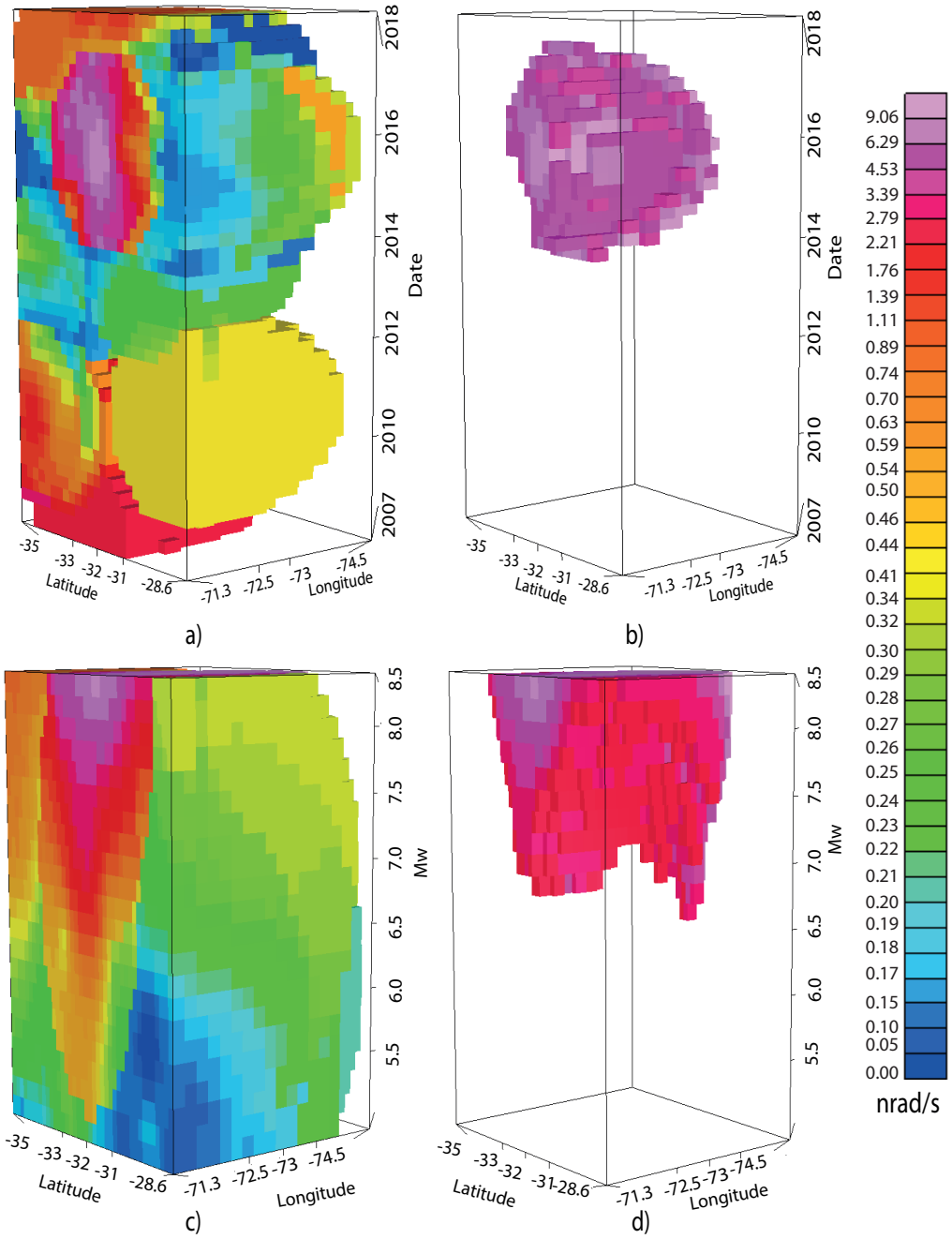

Figure 5: Timeline and Seismic Moment modeling for Central zone of Chile. In Figs. 5a) and 5b) the coordinates are given by Longitude, Latitude and the time is the vertical axis. In Figs. 5c) and 5d) the vertical axis is the seismic moment.

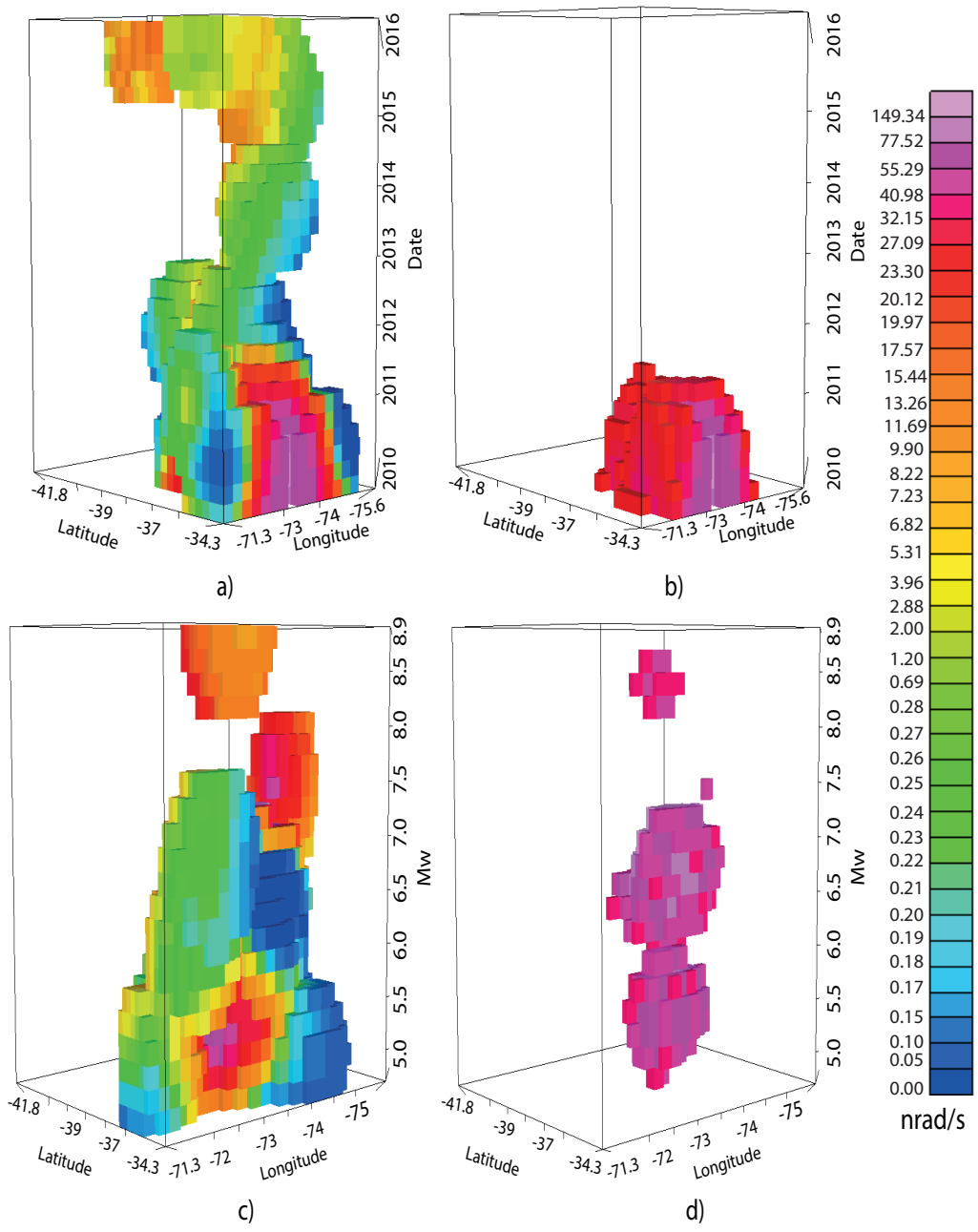

Figure 6: Timeline and Seismic Moment modeling for Southern zone of Chile. In Figs. 6a) and 6b) the coordinates are Longitude, Latitude and the time is the vertical axis. In Figs. 6c) and 6d) the vertical axis is the seismic moment.

We remark the fact that the results from the 2D and 3D models show a high value of VRR in seismic events with magnitudes lower than M_w7.0. In order to describe and understand further that phenomena, we compare the data of VRR as a function of M_w in each area (Northern zone of Chile, Central zone of Chile and Southern zone of Chile). These results are shown in Figs. 7, 8 and 9.

In Fig. 7 the large earthquake of 1st April 2014 with M_w8.2 shows a VRR of 3.7 nrad/s. On the other hand, there are two events near Tocopilla city, the first one is on 14th November 2007 with M_w7.7 and VRR of 1.93 nrad/s and the second one occurred on 26th December 2007 with M_w7.7 and VRR of 1.26 nrad/s. Finally, there are two events of M_w5.2 and M_w6.6 occurred on 6th April 2014 with 2.6 nrad/s and 2.2 nrad/s both related to the aftershocks of Iquique 2014. In Fig. 8 the event of 16th September 2015 with M_w8.3 shows a VRR of 9.05 nrad/s. On the other hand, there is an event on the 1st September 2015 with M_w7.1 and a VRR of 9.05 nrad/s. In Fig. 9 the event of 27th February 2010 with M_w8.8 shows a VRR of 17.4 nrad/s. On the other hand, there is a seismic event of M_w6.6 on 5th March 2010 with VRR of 172.1 nrad/s and a second seismic event of M_w5.5 on 19th March 2010 with a VRR of 227.79 nrad/s.

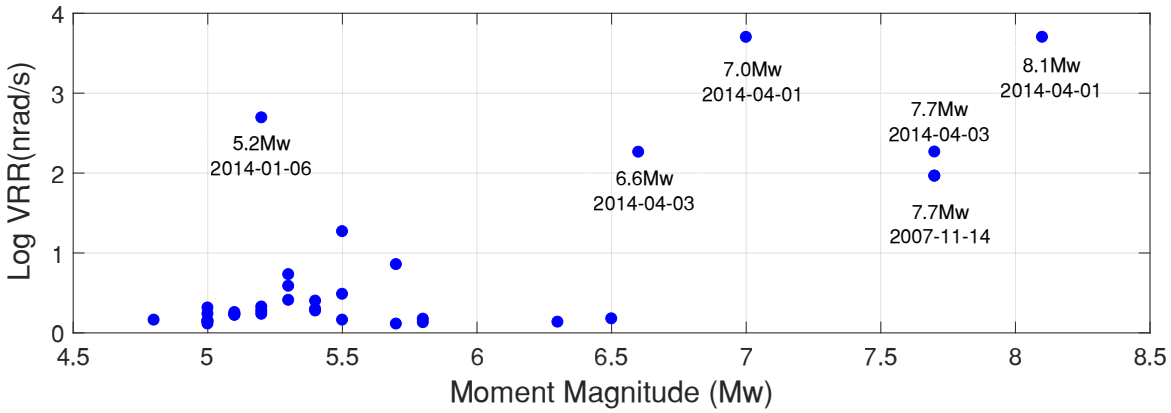

Figure 7: Correlation between VRR versus M_w for the seismic events registered in the Northern zone of Chile.

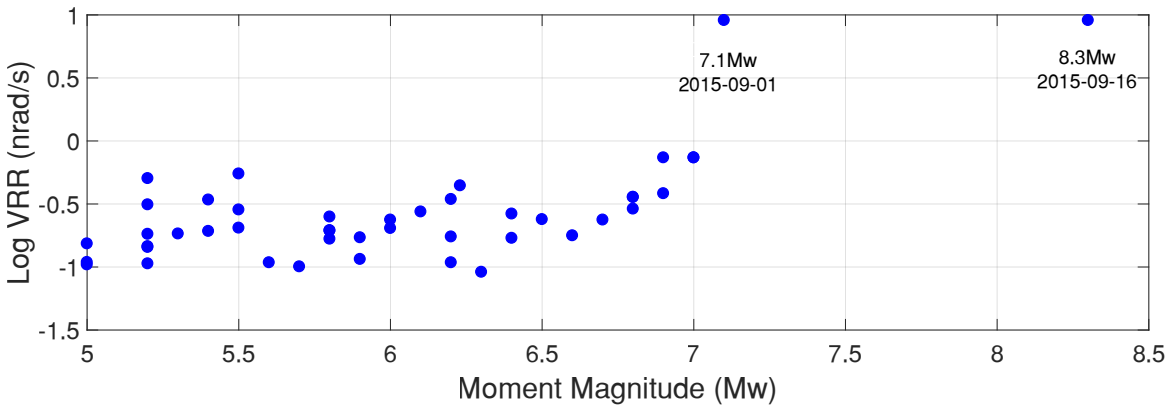

Figure 8: Correlation between VRR versus M_w for the events registered in the Central zone of Chile.

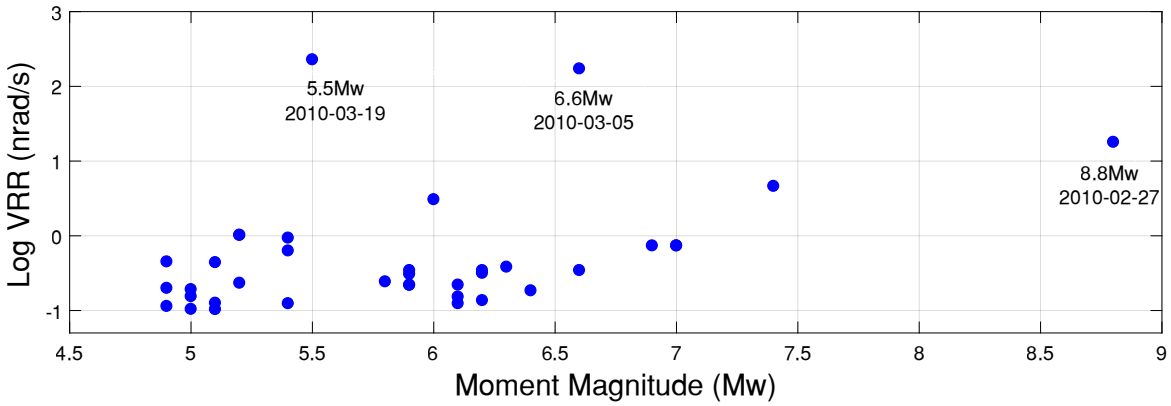

Figure 9: Correlation between VRR versus the moment magnitude M_w for the seismic events registered in the Southern zone of Chile.

The SR correlation gives the values showed in Table I:

Area	P_{sp}
Northern	0.4241
Central	0.5373
Southern	0.4241

Table I: SR correlation computed for Figs. 7, 8 and 9 from rotational seismic events measured in Chile between years 2007 and 2018.

5. DISCUSSION

The results obtained from the interpolation data measured by the BWLRAS observatory suggest that the geological subduction zone between Nazca and South America plates along Chile, as show in Fig. 3, has important values of VRR between northern, central and southern area.

In particular the VRR map from the Northern zone of Chile, Fig. 3a), shows seismic events with VRR of 1.03 nrad/s, while the map for seismic data measured in the Southern zone of Chile shows two VRR hot spots into the subduction zone (Fig. 3c)), specifically on the neighborhood of the Maule 2010 main event.

The temporal and Seismic Moment evolution of rotational seismic velocities between years 2007 and 2018 in each area shows an interesting result. The Northern area shows an event occurred on 26 December 2007 with a VRR of 1.93 nrad/s at 151 Km of depth with $Mw5.5$, Fig. 4b). This particular seismic event had a similar value of VRR compared with the $Mw8.2$ event occurred the 1st April 2014 which had a VRR of 2.8 nrad/s. For the Central zone of Chile, the VRR evolution in time and seismic moment shows that there are two seismic events on 1th September 2015 and 16th September 2015, Fig. 5b) with magnitudes $M_w7.1$ and $M_w8.3$ which had a VRR of 9.05 nrad/s each one. The Southern zone of Chile, Fig. 6b), has the maximum values of VRR compared with the Northern and Central zones. In particular, there are events with magnitudes of $M_w4.9$ and $M_w5.5$ with values of VRR of 30 nrad/s and 87 nrad/s, respectively.

The comparison between VRR and the moment magnitude M_w for the events occurred in Chile, Figs. 7, 8 and 9, suggests that the VRR does not have a direct relationship between the seismic energy released by the seismic events. We note that there are events with magnitude lower than $M_w7.0$ with a high value of VRR and there are events with a large magnitude (greater than $M_w8.0$) with a low value of VRR. That fact is clear in the Southern zone of Chile, Fig. 9 where the events of 5th March 2010, with $M_w6.6$ and the 9th March 2010 with $M_w5.5$ have a VRR value of 172.1 nrad/s and 227.79 nrad/s respectively, which are significantly greater than the VRR value of the main event of February 27, 2010 of M_w 8.8. This evidence is in accordance with the results

of Vicencio et al.,[16] where rotational ground motion for building, during an earthquake, does not increase with the period of the structure. In this sense, we remark the importance of incorporating rotational sensors to the current seismological networks in Chile for a full characterization of ground motions during earthquakes.

6. CONCLUSION

The database of the BWLRAS observatory in Germany has allowed us to characterize the seismic events occurred in Chile between years 2007 a 2018 from the rotational point of view. This characterization allows us to determine that the VRR yields information complementary to the traditional seismological models, through the 2D interpolation of three active seismic zones in Chile.

On the other hand, the results of the application of the 3D Timeline and Seismic Moment model suggest that there is not direct correlation between the VRR and the moment magnitude M_w. This could mean that there is not a correlation between VRR and the seismic energy released. Also, it is possible to remark that the main events of Tocopilla 2007, Maule 2010 and Iquique 2014 had aftershocks with higher VRR compared with their main events. Meanwhile, days before of the main event of Illapel 2015, there was an earthquake of M_w7.1 with the same VRR value of the large earthquake in Illapel 2015. This result suggests that the VRR and the rotational seismic parameters could give more information related to the geodynamics of the plates and/or the Earth's layers in terms of the torsion exerted during an earthquake.

This study opens a new path to analyze seismic data sets, and it suggests the development of physical models that allow a better characterization of the rotational seismic data in order to verify the results found in the present analysis. Given the paleo-seismological context in which Chile is embedded, it has been proposed to incorporate optical sensors to measure the rotational parameters in seismic waves for local events (through local seismic networks), in order to expand this analysis. The last proposal is supported based on the need to gather more information from rotational seismic waves in the near-field and far-field.

7. ACKNOWLEDGMENT

Authors acknowledge to Rotational Seismology Event Database from Rotational Motions in Seismology (ROMY) project where all data were obtained and it is available at https://rotations-database.geophysik.uni-muenchen.de/. Also authors acknowledge to R.M, P.S, A.M, and I.C. for useful comments and discussions. This work was supported in part by FONDECYT Grants N° 11160452 and 11190078, CONICYT Grant PAI 77180003, and Programa ICM Millennium Institute for Research in Optics (MIRO). Authors acknowledge as well the open database from BWLRAS.

REFERENCES

[1] S. Ruiz, R. Madariaga, "Historical and recent large megathrust earthquakes in Chile," *Tectonophysics* **733**, 37 (2018).

[2] C. Vigny, A. Socquet, S. Peyrat, J.-C. Ruegg, M. Métois, R. Madariaga, S. Morvan and M. Lancieri, R. Lacassin, J. Campos, D. Carrizo, M. Bejar-Pizarro, S. Barrientos, R. Armijo, C. Aranda, M.-C. Valderas-Bermejo, I. Ortega, F. Bondoux, S. Baize, H. Lyon-Caen, A. Pavez, J. P. Vilotte, M. Bevis, B. Brooks, R. Smalley, H. Parra, J.-C. Baez, M. Blanco, S. Cimbaro and E. Kendrick, "The 2010 Mw 8.8 Maule Megathrust Earthquake of Central Chile, Monitored by GPS," *Science* **332**, 6036 (2011).

[3] M. Metois, C. Vigny and A. Socquet, "Interseismic coupling, megathrust earthquakes and seismic swarms along the Chilean subduction zone," *Tectonophysics* **137**, 1431 (2016).

[4] M. Metois, A. Soquet, C. Vigny, D. Carrizo, S. Peyrat, A. Delorme, E. Maureira, M.-C. Valderas-Bermejo and I. Ortega, "Revisting the North Chile seismic gap segmentation using GPS-derived interseismic coupling," *Geophys. Jornal Int.* **194**, 1283 (2013).

[5] W.R.McCann, S.P. Nishenko, L.R. Sykes and J. Krause, "Seismic gaps and plate tectonics: Seismic potential for major boundaries," *Pure and Appl. Geophys.* **117**, 1082 (1979).

[6] S. Nishenko, "Seismic potential for large and great interplate earthquakes along the Chilean and Southern Peruvian margins of South America: a quantitative reappraisal," *J. Geophys. Res.* **90**, 3589 (1985).

[7] D. Melnick, M. Moreno, J. Quinteros, J.C. Baez, Z. Deng, S. Li, O. Oncken, "The super-interseismic phase of the megathrust earthquake cycle in Chile," *Geophys. Res. Lett.* **44**, 784 (2017).

[8] D. Comte and M. Pardo, "Reapraisal of great historical earthquakes in the northern Chile and southern Peru sesmic gaps," *Nat. Hazards* **4** (1991).

[9] Igel, H., Cochard, A., Wassermann, J., Flaws, A., Schreiber, U., Velikoseltsev, A., and Pham Dinh, N., "Broad-band observations of earthquake-induced rotational ground motions," *Geophysical Journal International* **168**(1), 182–196 (2007).

[10] Aki, K. and Richards, P. G., [*Quantitative Seismology, 2nd Ed.*], University Science Books (2002).

[11] Igel, H., Schreiber, U., Flaws, A., Schuberth, B., Velikoseltsev, A., and Cochard, A., "Rotational motions induced by the m8.1 tokachi-oki earthquake, september 25, 2003," *Geophysical Research Letters* **32**(8) (2005).

[12] Salvermoser, J., Hadziioannou, C., Hable, S., Chow, B., Krischer, L., Wassermann, J., and Igel, H., "An event database for rotational seismology," in [*EGU General Assembly Conference Abstracts*], *EGU General Assembly Conference Abstracts* **18**, EPSC2016–4042 (Apr. 2016).

[13] Pancha, A., Webb, T. H., Stedman, G. E., McLeod, D. P., and Schreiber, K. U., "Ring laser detection of rotations from teleseismic waves," *Geophysical Research Letters* **27**, 3553–3556 (2000).

[14] Nigbor, R. L., "Six-degree-of-freedom ground-motion measurement," *Bulletin of the Seismological Society of America* **84**, 1665–1669 (10 1994).

[15] D.Trifunac, M., "75th anniversary of strong motion observation: historical review," *Soil Dynamics and Earthquake Engineering* **29**(4), 591 – 606 (2009).

[16] Vicencio, F. and Alexander, N. A., "A parametric study on the effect of rotational ground motions on building structural responses," *Soil Dynamics and Earthquake Engineering* **118**, 191 – 206 (2019).

[17] Stedman, G. E., "Ring-laser tests of fundamental physics and geophysics," *Reports on Progress in Physics* **60**, 615–688 (June 1997).

[18] William. H. K. Lee1, John R. Evans, B.-S. H. C. R. H. C.-J. L. C.-C. L. and Nigbor, R. L., [*Measuring rotational ground motions in seismological practice*], Deutsches GeoForschungsZentrum GFZ (2012).

[19] Schreiber, K. U., Klügel, T., Velikoseltsev, A., Schlüter, W., Stedman, G. E., and Wells, J.-P. R., "The large ring laser g for continuous earth rotation monitoring," *Pure and Applied Geophysics* **166**, 1485–1498 (Sep 2009).

[20] Velikoseltsev, A., Schreiber, K. U., Yankovsky, A., Wells, J.-P. R., Boronachin, A., and Tkachenko, A., "On the application of fiber optic gyroscopes for detection of seismic rotations," *Journal of Seismology* **16**, 623–637 (Oct. 2012).

[21]

[22] Smith, W. H. F., "Gridding with continuous curvature splines in tension," *Geophysics* **55**, 293 (Mar. 1990).

[23] Witteveen, J. and Bijl, H., "Explicit mesh deformation using inverse distance weighting interpolation," *19th AIAA Computational Fluid Dynamics* (2009).

[24] Zhang, W.-Y., Wei, Z.-W., Wang, B.-H., and Han, X.-P., "Measuring mixing patterns in complex networks by Spearman rank correlation coefficient," *Physica A Statistical Mechanics and its Applications* **451**, 440–450 (June 2016).